

Article

Poly(ϵ -caprolactone)–Ionic Liquid Composite as Piezoionic Mechanical Sensor

Giovanna Di Pasquale ¹, Salvatore Graziani ^{2,*} , Alberta Latteri ³, Antonino Pollicino ^{3,*}  and Carlo Trigona ^{2,*}

¹ Dipartimento di Scienze Chimiche (DSC), University of Catania, Viale Andrea Doria 6, 95125 Catania, Italy; giovanna.dipasquale@unict.it

² Dipartimento di Ingegneria Elettrica Elettronica e Informatica (DIEEI), University of Catania, Viale Andrea Doria 6, 95125 Catania, Italy

³ Dipartimento di Ingegneria Civile e Architettura (DICAr), University of Catania, Viale Andrea Doria 6, 95125 Catania, Italy; alatteri@unict.it

* Correspondence: salvatore.graziani@unict.it (S.G.); apollicino@unict.it (A.P.); carlo.trigona@unict.it (C.T.)

Abstract: In recent years, the issue related to electronic waste production has been gaining prominence. One of the approaches considered to limit the impact of e-waste on the environment involves the development of biodegradable electronic devices or devices that dissolve in the environment at the end of their life cycle. In this study, we present the preliminary results related to the creation of a sensor that could meet both criteria. The device was constructed using a composite material obtained by impregnating a membrane of polycaprolactone (a biodegradable polymer) with 1-Ethyl-3-Methylimidazolium tetrafluoroborate (a water-soluble ionic liquid), which was coated with a conductive silver-based varnish. Leveraging the piezoionic effect, the device has been proven to function as a vibration sensor with a sensitivity of approximately 1.9×10^{-5} V/mm and a resolution of about 0.15 mm.

Keywords: poly(ϵ -caprolactone); electrospinning; imidazolium ionic liquid; piezoionic composite; mechanical sensor



Citation: Di Pasquale, G.; Graziani, S.; Latteri, A.; Pollicino, A.; Trigona, C. Poly(ϵ -caprolactone)–Ionic Liquid Composite as Piezoionic Mechanical Sensor. *Appl. Sci.* **2024**, *14*, 1085. <https://doi.org/10.3390/app14031085>

Academic Editor: Manoj Gupta

Received: 24 December 2023

Revised: 23 January 2024

Accepted: 24 January 2024

Published: 27 January 2024



Copyright: © 2024 by the authors. Licensee MDPI, Basel, Switzerland. This article is an open access article distributed under the terms and conditions of the Creative Commons Attribution (CC BY) license (<https://creativecommons.org/licenses/by/4.0/>).

1. Introduction

Electronic waste (e-waste) production is caused by discarded electronic devices and electrical equipment that have reached the end of their useful life or are no longer wanted by their owners. E-waste encompasses a wide range of electronic products, from consumer electronics, like smartphones and laptops, to large appliances, industrial equipment, and more. The proliferation of electronic devices in modern society has led to a significant increase in an e-waste generation. Rapid technological advancements and shorter product lifespans contribute to this issue and determine substantial environmental challenges. Many electronic devices contain hazardous materials such as lead, mercury, cadmium, and flame retardants [1]. When not properly managed, these toxins can leach into the soil and water, causing pollution, harm to ecosystems, and health risks for both humans and animals. Extended producer responsibility (EPR) programs hold manufacturers responsible for the end-of-life management of their products [2]. These programs incentivize manufacturers to design products with recycling and environmental impact in mind.

A way that can help mitigate the environmental and health risks associated with e-waste and promote a more sustainable approach to electronic device usage and disposal has been adopted through transient electronics [3–5]. Transient electronics is a captivating and cutting-edge field that has garnered significant attention in recent years within the realm of advanced materials and electronics research. This emerging technology promises groundbreaking applications by designing electronic systems that, unlike their conventional counterparts, intentionally degrade and disappear after fulfilling their purpose. Drawing inspiration from the natural world, where everything has a limited lifespan, transient

electronics emulate this ephemeral concept, offering a wide array of potential applications in medicine, environmental monitoring, and data security. The literature surrounding transient electronics is a rich tapestry of scientific exploration, spanning disciplines such as materials science, electronics, and bioengineering [6–10]. In the intriguing world of transient electronics, researchers endeavor to create devices that can exist only briefly, leaving no trace behind, thereby challenging our conventional notions of electronics.

In this scenario, biodegradable polymers occupy a prominent place, and among them polycaprolactone (PCL), a biodegradable and biocompatible polyester with various applications, has found its use in sensors due to its unique properties [4,11,12]. Due to its flexibility and ease of processing, PCL has been used in producing strain gauges [13], pressure sensors [12], biomechanical sensors [14], tactile sensors [15], biodegradable sensors, and smart fabrics [16]. The use of PCL in mechanical sensors offers versatility, biocompatibility, and biodegradability, making it a promising material for a wide range of sensing applications in industries such as healthcare, robotics, and environmental monitoring. Its ability to be tailored to specific mechanical and environmental requirements makes it an attractive choice for sensor development.

PCL has been widely used in the realization of mechanical sensors due to its favorable mechanical properties and biocompatibility [17–20]. PCL exhibits high mechanical strength, making it suitable for applications in tissue engineering and regenerative medicine [17,19,20]. It is well tolerated *in vivo* and has been used in various biomedical applications [18]. PCL also degrades at a rate compatible with bone regeneration, making it suitable for bone tissue engineering [19].

In the field of bionanocomposites, PCL has been grafted onto microfibrillated cellulose to enhance the mechanical properties of the composite material [21]. The grafting of PCL onto cellulose allows for the preparation of thermoformable bionanocomposites with good mechanical strength [21]. Furthermore, PCL has been utilized in the fabrication of 3D printed mechanochromic materials, which can change color in response to mechanical stimuli [22]. PCL containing a chain-centered spiropyran has been 3D printed and explored for its mechano-responsive characteristics, demonstrating its potential for use in prototype force sensors [22]. In the context of nanofiber scaffolds, electrospun PCL nanofibers have been combined with bioceramics to improve the mechanical characteristics of the scaffold and enhance the osteogenic differentiation of stem cells [23]. This combination of PCL nanofibers and bioceramics has been used to increase the mechanical strength of the nanofibrous scaffold [23]. Overall, PCL has been extensively utilized in the realization of mechanical sensors due to its favorable mechanical properties, biocompatibility, and ability to be incorporated into various composite materials and scaffolds.

Ionic liquids (ILs) are a class of liquid salts that are composed entirely of ions, which comprise both positively charged cations and negatively charged anions. Unlike traditional salts like sodium chloride, which have high melting points and are typically solid at room temperature, ionic liquids remain in a liquid state at or near room temperature. They exhibit a unique combination of properties that make them valuable in various scientific, industrial, and technological applications [24–27]. They have excellent thermal stability, resisting decomposition at high temperatures, low vapor pressures (they do not readily evaporate, making them useful in closed systems), and properties that can be finely tuned by selecting specific cations and anions, thus allowing for customization based on the desired application. Moreover, many ionic liquids are non-flammable or have low flammability, making them safer than some organic solvents.

The term “piezoionic effect” denotes a phenomenon observed, for instance, when blending a polymer matrix with an ionic liquid. In such materials, mechanical deformation or stress can induce ion movement, leading to ionic conductivity. Though not as widely acknowledged as conventional piezoelectric materials, recent research [28,29] has brought attention to the piezoionic effect. These sensors have garnered interest for a range of uses, such as in human–machine interfaces for medical robotics [30], as wearable sensors to track human movements [31], and as strain sensors as well as energy harvesters [32]. Their dis-

tinct benefits include self-powered signal generation and the ability to detect the direction of an applied load, positioning them as compelling options for wearable electromechanical sensing applications [33]. The piezoionic effect creates ion concentration variances under pressure, resembling the signal production and transmission in biological systems like cell membranes. This makes them well suited for biomimetic sensor applications [34]. Additionally, piezoionic sensors have been proven to operate effectively across a broad spectrum of both steady and fluctuating applied pressures, making them capable of capturing physiological data in various static and dynamic scenarios [35]. The piezoionic effect closely resembles the redistribution of the ion concentration in natural mechanoreceptor cell membranes when they are externally stimulated, offering a promising pathway for developing biomimetic mechanoreceptors [36].

Electrospinning is a versatile and widely used technique for producing polymeric membranes with a range of applications, including filtration, tissue engineering, drug delivery, and more [37–39]. It involves the use of an electric field to create ultrafine polymer fibers that are collected on a substrate to form a membrane. Electrospinning offers precise control over membrane properties, including fiber diameter and pore size, making it a valuable technique for tailoring membranes for specific applications.

In recent years, our research has focused on the study of “green” composites comprised of bacterial cellulose and ionic liquids. We have demonstrated that these composites generate electrical signals when subjected to mechanical strain, thus functioning as sensors, due to the piezoionic effect generated by the movement of the components of the IL [40,41]. Furthermore, these systems can also function as fractional capacitors, thereby paving the way for the possibility of eco-friendly electronics [42].

In this work, we present the preliminary results obtained by extending our research to the use of a widely available, as well as biocompatible and biodegradable, polymeric material such as PCL. In order to create our sensor, PCL membranes, which were obtained through electrospinning, were impregnated with an IL and coated with a conductive silver-based varnish. The resulting composites were characterized morphologically, chemically and electromechanically.

2. Materials and Methods

Poly(ϵ -caprolactone) (PCL) ($M_n = 45,000 \text{ g mol}^{-1}$), chloroform (CHCl_3), and dimethylformamide (DMF), which were used for the electrospinning process of the polymer, were furnished by Merck/Sigma Aldrich KGaA (Darmstadt, Germany) and were used without purification. 1-Ethyl-3-Methylimidazolium tetrafluoro borate (EMIMBF_4) was purchased from Fisher Scientific Italia/Alpha Aesar (Segrate, Italy). The conductive silver-based varnish spray used as the electrode was furnished by Tifoo (Regensburg, Germany). Electrospinning was carried out by using a commercially available apparatus (Starter Kit 40 kV Web, Linari Nanotech srl, Pisa, Italy), comprised of a high-voltage power supply, a syringe pump, a syringe, a stainless steel blunt-ended needle connected with the power supply electrode, and a grounded drum collector covered with aluminum foil. PCL electrospun scaffolds were produced by dissolving the PCL at a concentration of 20% w/v in a solution of CHCl_3/DMF (4:1). The polymer solution was poured into a 20 mL syringe equipped with 21-gauge needle (inner diameter = 0.8 mm). A voltage of 15 kV was applied through a high-voltage power supply. The perpendicular distance between the syringe tip and the grounded drum collector was set at 15 cm. The flow rate of 3 mL/h was controlled through the pump speed. The electrospinning process was carried out at 25 °C and at 57% relative humidity.

To fabricate the devices, electrospun PCL membranes (2 cm \times 5 cm) were cut, dried in an oven at 40 °C, soaked with EMIMBF_4 for 24 h, and left again in an oven for 24 h at 40 °C. PCL/ EMIMBF_4 /Ag devices were fabricated by spraying a conductive varnish on both sides of the membrane twice. After every deposition, the membranes were dried in an oven for 5 min ($T = 40 \text{ }^\circ\text{C}$). The device thickness was determined using a caliper (accuracy $\pm 1 \text{ }\mu\text{m}$).

Characterization Methods

The IL and silver-based varnish were determined by weight percentage content using an analytical balance. Thermogravimetric analyses (TGAs) have been carried out through a Shimadzu (Kyoto, Japan) model DTG-60 instrument. TGA curves have been recorded at a heating rate of $20\text{ }^{\circ}\text{C min}^{-1}$, under a nitrogen flux (20 mL min^{-1}), and from $35\text{ }^{\circ}\text{C}$ to $700\text{ }^{\circ}\text{C}$. Analyzed sample mass varied between 8.0 mg and 11.0 mg. Scanning electron microscopy (SEM) micrographs have been obtained using a SEM EVO (Zeiss, Cambridge, UK) instrument equipped with an energy dispersive X-ray microanalysis (EDX) facility. The analyses were performed by setting a high electron beam voltage (EHT) of 20 kV and using a LaB₆ (Lanthanum Hexaboride) emitter as the electron source. To carry out the SEM analysis, the samples were gold-sputtered with a thin gold film deposited through a sputtering process that was carried out using an Agar Sputter Coater AGB7340 spray coating machine (Agar Scientific, Stansted UK). XPS spectra were recorded using a VG Microtech Ltd (Uckfield, UK) spectrometer with a CLAMII analyzer. The X-ray source (Mg K α , 1253.6 eV) worked at 200 kV and 10 mA at a pressure of $<2 \times 10^{-8}$ Torr, a pass energy of 100 eV, and a take-off angle 45° . Binding energies were referenced according to the C–H level at 285.0 eV. Dynamical mechanical analysis (DMA) was carried out using a 2000 TA DMA produced by Triton Technology Ltd. (London, UK). The frequency dependence of the membrane modulus has been evaluated in single cantilever mode by applying a sinusoidal force to a rectangular sample in the range 0.1–50 Hz at the working temperature $T = 25\text{ }^{\circ}\text{C}$.

The investigation into the piezoionic PCL sensor's response to mechanical vibrations was conducted on rectangular samples ($1\text{ cm} \times 5\text{ cm}$ – $170\text{ }\mu\text{m}$ thick) with a suitable experimental setup. This setup comprised instruments to gauge the sensor's electrical signals under vibration and a shaker to apply controlled kinetic movement (Figure 1). To analyze the mechano-electrical transduction behavior of the PCL-based device, the utilized configuration included the equipment as follows:

- TIRA GmbH (Schalkau, Germany) S51110 Shaker: Used to impress motion in the sensor arranged as a cantilever beam.
- Agilent Infiniium MSO9064A Digital Oscilloscope (Agilent, Santa Clara, CA, USA): Equipped with an 8-bit resolution and a maximum input sensitivity of 5 V/div (with a $1\text{ M}\Omega$ load). It was employed for signal visualization and acquisition.
- Keysight 33220A Signal Generator (Keysight Technologies Italy S.r.l., Milano, Italy): Used to drive the shaker, thereby enabling precise control over mechanical vibrations.
- Baumer 12U6460/S35A Laser Sensors ($\times 2$) (Baumer Italia S.r.l. Assago, MI, Italy): These sensors, with a resolution of approximately $2\text{ }\mu\text{m}$ and adjustable sensitivity, measured vibration at the anchor and monitored tip displacement.
- Accelerometer PCB333B40-SN51174 (PCB Piezotronics, Depew, NY, USA): Mounted on the shaker's moving plate, this accelerometer served as a reference with a resolution of a 0.0005 m/s^2 root mean squared value (RMS) and a sensitivity of about $51.0\text{ mV/(m/s}^2)$.

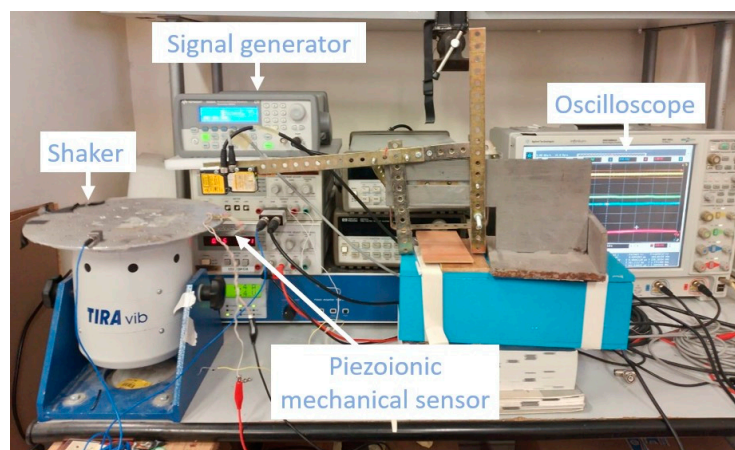


Figure 1. Photograph of the experimental setup.

3. Result and Discussion

The aim of our research was to develop a device capable of detecting vibrations by harnessing the piezoionic effect generated through the creation of a composite PCL/ionic liquid. The produced three-layer device was composed of a PCL electrospun scaffold soaked in EMIMBF₄ and placed between two silver-based electrodes (Figure 2).

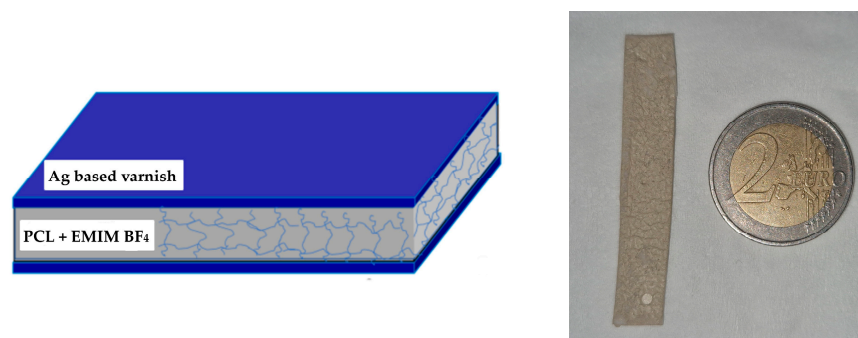


Figure 2. Structure and photograph of the device.

We focused our research on a widely used biodegradable polymer such as PCL. Concerning the choice of the IL, we are aware that there are ILs that are more environmentally friendly than EMIMBF₄. But, we have chosen EMIMBF₄ in this preliminary phase to put ourselves in conditions where the ionic liquid ensures high ionic conductivity. Our recent studies on a bacterial cellulose/IL composite [43] have demonstrated that, compared with other imidazolium-based ionic liquids or choline-derived ones, EMIMBF₄ provides a better performance. This is attributed to the fact that, as reported in the literature, its specific conductivity values are among the highest, reaching 13 mS/cm [44].

The weight percentage abundance of each component, calculated by weighing the samples after each stage of their preparation, was found to be 39% PCL by weight, 58.5% EMIMBF₄ by weight, and 2.5% conductive varnish by weight. As is known, electrospinning results depend on many different factors, which, among others, can usually be divided into solution properties such as polymer concentration, molecular weight, viscosity, surface tension, solution vapor pressure, electrical conductivity, and dielectric constant. They can also be divided into process parameters like flow rate, spinning voltage, configuration of electrodes, and distance between the electrodes, as well as environmental parameters such as temperature and humidity. These factors affect the initiation and stability of the electrospinning process and, ultimately, the morphology and properties of the fibers.

In our experiment the combination of the used solvent mixture (CHCl₃/DMF), the distance between the syringe tip and the grounded drum collector, and the flow rate of 3 mL/h produced a scaffold where fibers in the presence of flat polymer ribbons are present (SEM micrograph of Figure 3 on the left). The soaking of the membrane with EMIMBF₄ resulted in a modification of membrane morphology, as shown through the SEM micrograph (Figure 3 on the right) in which the IL, filling the pores of the PCL scaffold, is present as a continuous phase that wets the fibers and ribbons.

To determine the actual presence of EMIMBF₄ on the sample surface, we analyzed the composition of the soaked PCL surface through X-ray photoelectron spectroscopy (XPS). The wide scan shown in Figure 4 evidenced that carbon, oxygen, boron, nitrogen, and fluorine are present on the sample surface. The peaks centered at about 187 (B_{1s}), 400 (N_{1s}), and 685 eV (F_{1s}), which derive from emerging on the surface of the IL.

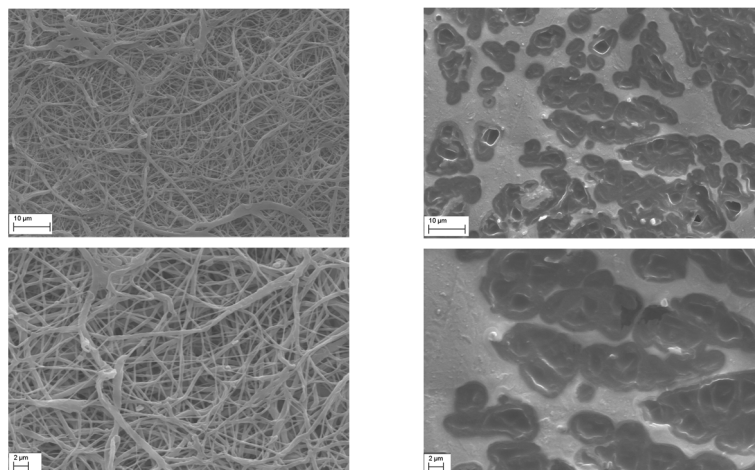


Figure 3. SEM micrographs showing the morphology of the membrane as electrospun (left) and soaked with the EMIMBF₄ IL (right).

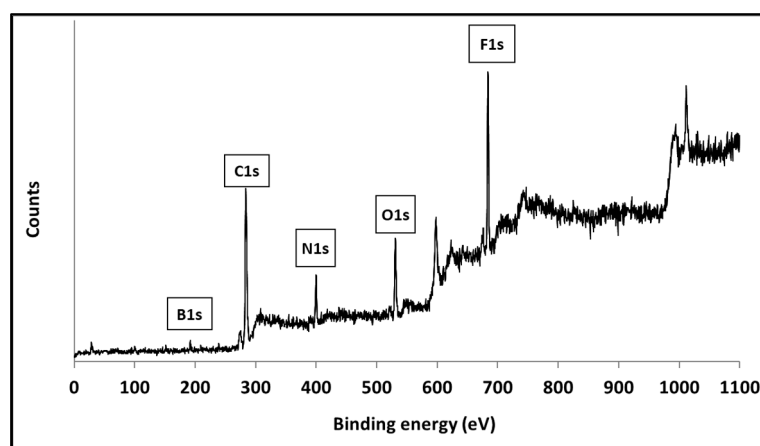


Figure 4. Wide scan of the XPS spectrum of the surface of the PCL/EMIMBF₄ sample.

The ATR FTIR registered in the range 4000–650 cm^{-1} (Figure 5) showed that the device presents the IR characteristic peak of PCL and EMIMBF₄ on its surface. The broad peak centered at about 2945 cm^{-1} due to the alky chains, and the peak centered at about 1721 cm^{-1} due to the stretching of carbonyl group of the ester function, derive from the presence of PCL. Regarding EMIMBF₄ presence, the bands at 3165 and 3124 cm^{-1} are assigned to the C-H of imidazole ring, while the bands at 1576 and 1457 cm^{-1} are due to the imidazole ring skeleton's stretching vibration, and the broad peak at 1017 cm^{-1} is due to the C-H of the imidazole ring stretching vibration.

TGA of the PCL membrane confirmed that electrospinning did not produce any significant degradation of the polymer structure. In fact, as shown in Figure 6a where the temperature dependence of the PCL's weight loss is plotted, the DTG curve displays one main degradation process with a maximum weight loss rate observed at 425 °C and a shoulder at a lower temperature at ca. 335 °C, which are in agreement with what was reported in the literature [45]. These peaks in the DTG curve are the result of two consecutive steps in the degradation process, with the first one being due to the production of H₂O, CO₂, and 5-hexanoic acid, and the second one being due to there being ϵ -caprolactone (cyclic monomer) evolution in addition to the preceding compounds. Comparing the TGA and DTG curves of the PCL membrane (Figure 6a), EMIMBF₄ (Figure 6b), and the PCL membrane soaked with EMIM BF₄ (Figure 6c), it can be noted that the interaction of the IL with PCL determines a change in the maximum weight loss rate temperature of both PCL and the IL.

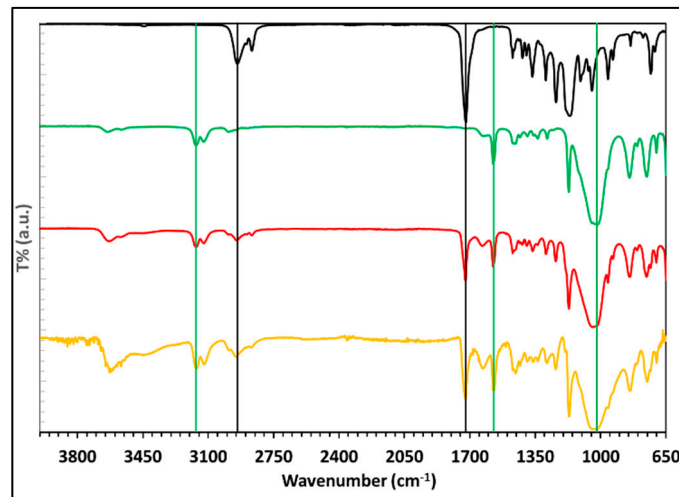


Figure 5. ATR FTIR spectra of PCL (black), EMIMBF₄ (green), PCL/EMIMBF₄ (red), and PCL/EMIMBF₄/Ag (yellow) samples.

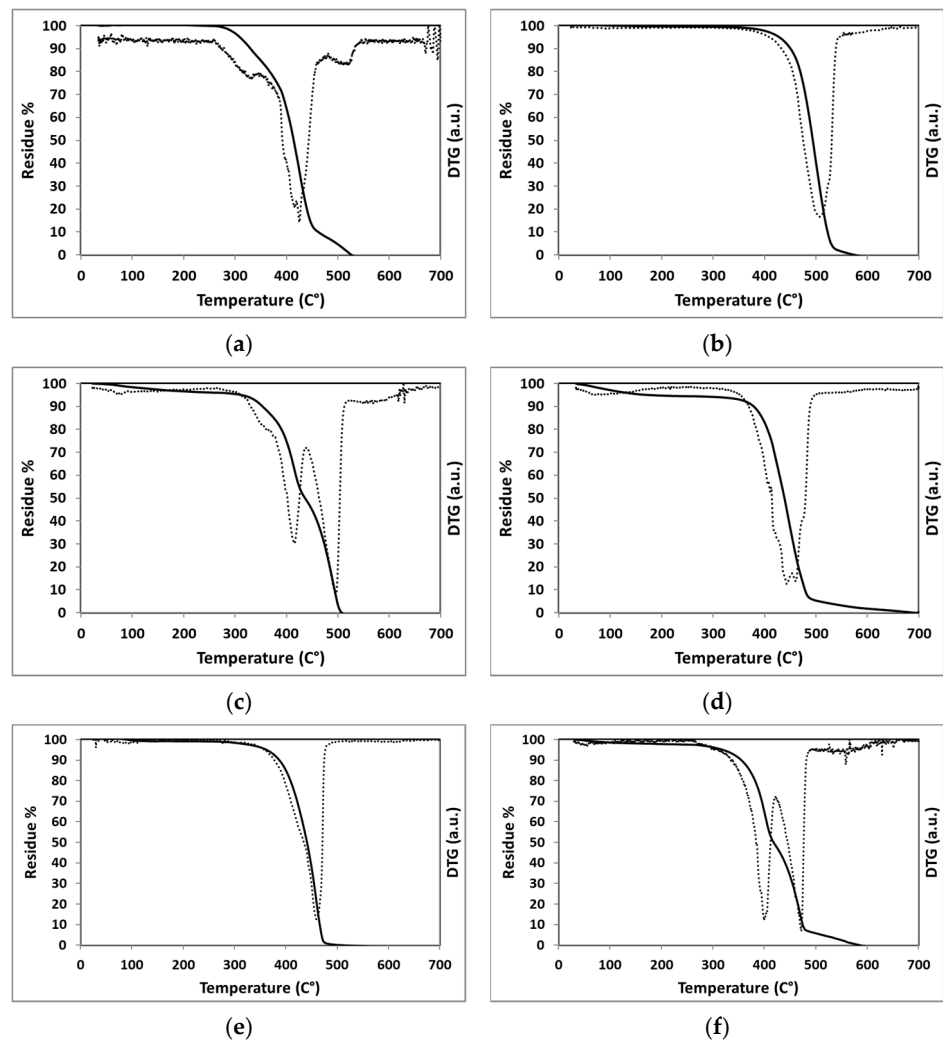


Figure 6. TGA (continuous line) and DTG (dashed line) plots of the PCL membrane as electrospun (a), EMIMBF₄ (b), the PCL membrane soaked with the EMIMBF₄ (c), and the soaked membrane coated with silver-based electrodes (d), EMIMBF₄ in static air with a ramp of 10 °C min⁻¹ (e), and the PCL membrane soaked with the EMIMBF₄ in static air with a ramp of 10 °C min⁻¹ (f).

In fact, in the case of PCL, there are still two main decomposition steps, but their maximum weight loss rates occur at 357 °C and 415 °C, respectively, while the maximum weight loss rate for EMIMBF₄ is at 497 °C instead of at 507 °C. The coating of the PCL/EMIMBF₄ composite through the deposition of the silver-based electrodes determines a modification of the DTG curve profile (Figure 6d) that is the result of the superposition of different contributions. There are the ones deriving from PCL degradation at lower temperatures and the one deriving from the maximum weight loss rate of EMIMBF₄ at higher temperatures, and between them a peak due to the maximum weight loss rate of the matrix in the silver varnish.

TGA can also provide an indication of the IL's stability under the specific conditions in which the device will be used. Our device is designed for use in ambient air and, accordingly, we conducted a TGA experiment in static air with a ramp of 10 °C min⁻¹. Upon comparing the resulting TGA curve with the preceding ones, as illustrated in Figure 6e, it becomes evident that the IL's weight loss occurs in a single step. However, the maximum weight loss rate is observed at a lower temperature (460 °C) compared with the previous condition (507 °C).

When examining the PCL/EMIMBF₄, the resulting DTG curve continues to display two main peaks in weight loss rates, which are centered at 400 °C and 472 °C, respectively. Notably, these peaks occur at lower temperatures compared with the observations made within a nitrogen atmosphere (at 415 °C and 497 °C, respectively).

Moreover, from the observation of the thermogravimetric analysis curves, it can be deduced that the ionic liquid used contains a negligible percentage of water, which is approximately 0.04% by weight. On the other hand, the final device contains a water content of about 3% by weight.

The obtained mechanical sensor is forecast to work in the low frequency domain. For this reason, we intended to study the viscoelastic properties of the devices in the range of 0.1–50 Hz at the working temperature of 25 °C. Measurements of the storage modulus (E') and the loss modulus (E'') were obtained and compared to determine the evolution of the mechanical properties from the crude PCL membrane to the final device. Obtained results at frequencies of 1, 10, and 50 Hz are reported in Table 1.

Table 1. Measurements of the storage modulus (E') and the loss modulus (E'') of the PCL membrane, PCL/EMIMBF₄, and PCL/EMIMBF₄/Ag.

		PCL	PCL/EMIMBF ₄	PCL/EMIMBF ₄ /Ag
E' (Pa)	1 Hz	9.8×10^5	1.2×10^6	6.6×10^8
	10 Hz	1.1×10^6	1.4×10^6	8.1×10^8
	50 Hz	1.6×10^6	1.5×10^6	9.8×10^8
E'' (Pa)	1 Hz	8.8×10^4	1.3×10^5	8.7×10^7
	10 Hz	8.9×10^4	1.9×10^5	1.3×10^8
	50 Hz	3.3×10^5	3.3×10^5	1.6×10^8

From the data reported in Table 1, it can be observed that the values of E' and E'' remain almost constant when transitioning from PCL to the PCL/EMIMBF₄ composite. However, due to the stiffness of the electrodes, in the case of the final device both the values of E' and E'' show an increase of two orders in magnitude. Furthermore, with the increase in frequency, as expected, the values of E' and E'' tend to slightly increase in a linear trend, thereby indicating the absence of peaks related to the activation of dissipative phenomena.

The comprehensive setup, described in the characterization section, enabled a thorough examination of the piezoionic PCL sensor's response to mechanical vibrations, yielding valuable insights into its mechano-electrical transduction behavior.

The study focused on analyzing signals in the time domain, as shown in Figure 7. Specifically, it concentrated on the sensor's output voltage under a fixed RMS vibration level

of approximately 1.4 mm RMS. The frequency varied from 5 Hz to 9 Hz in the sinusoidal kinetic source induced by the shaker.

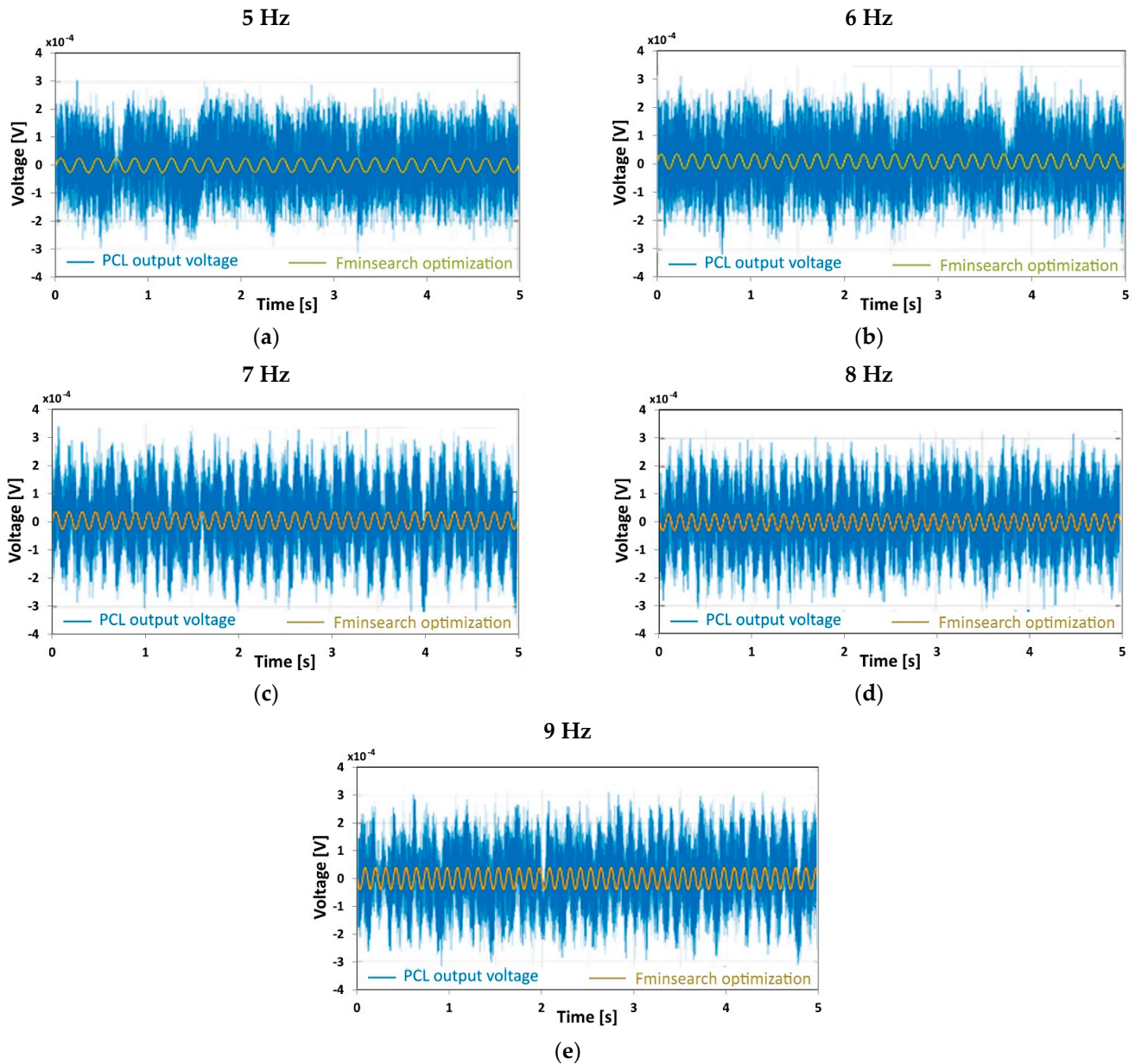


Figure 7. The evolution of the sensor's output voltage, maintaining a constant RMS vibration level of approximately 1.4 mm while changing the frequency, which is detailed below, at the values as follows: (a) at 5 Hz, (b) at 6 Hz, (c) at 7 Hz, (d) at 8 Hz, (e) at 9 Hz. Each graph showcases the approximation using a sinusoidal waveform obtained through the MATLAB® function of fminsearch.

The graph depicted the PCL's output voltage alongside a sinusoidal waveform generated using MATLAB®R2019a optimization. This process employed a nonlinear programming solver to minimize a quadratic deviation problem, executed through the fminsearch function. The waveforms illustrated significant attenuation of the output signal outside the resonance conditions.

The mechanical resonant frequency, evident at around 7 Hz as in Figure 8, illustrates the sensor's frequency response. A sinusoidal excitation ranging from 5 to 9 Hz was applied using the shaker. The mean output voltage and standard deviation at each frequency were measured using the aforementioned digital oscilloscope.

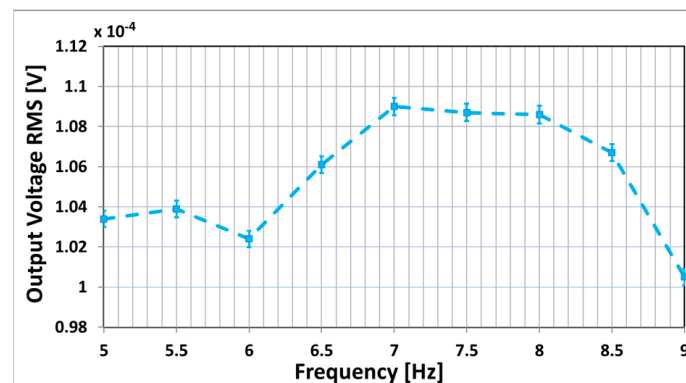


Figure 8. Output voltage of the sensor as a function of the frequency in the presence of a sinusoidal mechanical excitation maintaining a constant RMS vibration level of approximately 1.4 mm.

In particular, the graph shows the mean value and standard deviation of the measurements of the output voltage. Ten repetitions were conducted, and a time window of 5 s was considered for each repetition. Notably, a prominent peak aligned with the mechanical resonant frequency, which closely resembled the natural frequency of the device. For clarity, the dots have been connected for the ease of the eye.

Varied amplitudes of the input sinusoidal signal were utilized, and the output of the PCL-based piezoionic mechanical sensor was recorded. The vibration input was tracked through the laser at the anchor point.

Figure 9 presents the RMS output voltage of the device corresponding to different RMS mechanical vibrations. Each data point includes the mean value and the experimental standard deviation, which is derived from 10 repetitions. During the characterization, a time window of 5 s was considered for each repetition.

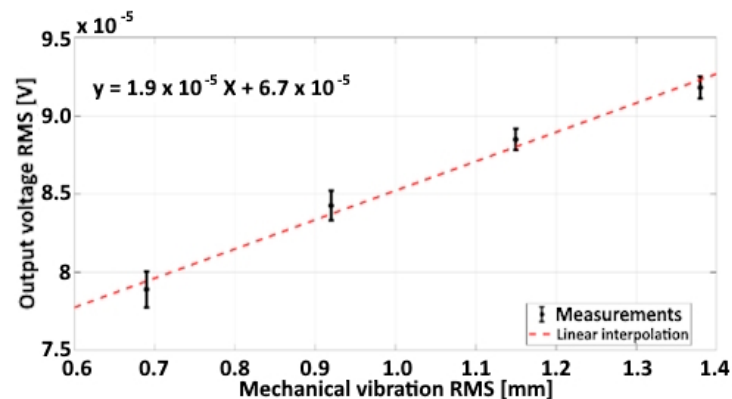


Figure 9. Characterization diagram of RMS output voltage of the device corresponding to different RMS mechanical vibrations.

Throughout these measurements, the PCL device exhibited a maximum deformation of approximately 4.4 mm (calculated as the difference between the two laser outputs at the tip and anchor, respectively) under a maximum mechanical vibration of about 1.4 mm. A sensitivity of roughly 1.9×10^{-5} V/mm was determined, and a resolution of about 0.15 mm was also estimated.

4. Conclusions

In conclusion, by utilizing a composite primarily composed of a biodegradable polymer and a water-soluble IL, we have developed a sensor that potentially falls within the field of transient electronics. The device, created by combining a PCL membrane produced through electrospinning, an ionic liquid to achieve a piezoionic effect, and a silver-based varnish for electrode production, does not exhibit significant changes in thermal stabil-

ity compared with the individual components. Dynamic mechanical analysis within the 0.1 to 50 Hz frequency range reveals the device's immunity to dissipative effects, holding a consistent modulus of approximately 8×10^8 Pa. Operating as a vibration sensor, it identifies resonances at roughly 7 Hz, offering a sensitivity of about 1.9×10^{-5} V/mm and a resolution of 0.15 mm.

The future development of this study will, among other things, focus on evaluating the impact of varying the concentration of the ionic liquid in the membrane on the viscoelastic behavior and sensor performance. Additionally, it aims to create devices based on biopolymers that are highly soluble in water, incorporating a piezoionic component derived from biological sources in combination with electrodes that are more biodegradable.

Author Contributions: The manuscript was written through the contributions of all the authors. All authors have read and agreed to the published version of the manuscript.

Funding: This research was funded by the project "Programma di ricerca di ateneo UNICT 2020-22 linea 2 PIA.CE.RI" SENSORS and by The European Union (NextGeneration EU) through the MUR-PNRR project SAMOTHRACE (ECS00000022).

Institutional Review Board Statement: Not applicable.

Informed Consent Statement: Not applicable.

Data Availability Statement: The data present in this study are available on request from the corresponding authors. The data are not publicly available due to restrictions on privacy.

Conflicts of Interest: The authors declare no conflicts of interest.

References

1. Robinson, B.H. E-waste: An assessment of global production and environmental impacts. *Sci. Total. Environ.* **2009**, *408*, 183–191. [[CrossRef](#)]
2. Kiddee, P.; Naidu, R.; Wong, M.H. Electronic waste management approaches: An overview. *Waste Manag.* **2013**, *33*, 1237–1250. [[CrossRef](#)] [[PubMed](#)]
3. Fu, K.K.; Wang, Z.; Dai, J.; Carter, M.; Hu, L. Transient Electronics: Materials and Devices. *Chem. Mater.* **2016**, *28*, 3527–3539. [[CrossRef](#)]
4. Li, R.; Wang, L.; Kong, D.; Yin, L. Recent progress on biodegradable materials and transient electronics. *Bioact. Mater.* **2018**, *3*, 322–333. [[CrossRef](#)] [[PubMed](#)]
5. Li, R.; Wang, L.; Yin, L. Materials and Devices for Biodegradable and Soft Biomedical Electronics. *Materials* **2018**, *11*, 2108. [[CrossRef](#)] [[PubMed](#)]
6. Teng, L.; Ye, S.; Handschuh-Wang, S.; Zhou, X.; Gan, T.; Zhou, X. Liquid Metal-Based Transient Circuits for Flexible and Re-cyclable Electronics. *Adv. Funct. Mater.* **2019**, *29*, 1808739. [[CrossRef](#)]
7. Yang, Q.; Lee, S.; Xue, Y.; Yan, Y.; Liu, T.; Kang, S.; Lee, Y.J.; Lee, S.H.; Seo, M.; Lu, D.; et al. Materials, Mechanics Designs, and Bioresorbable Multisensor Platforms for Pressure Monitoring in the Intracranial Space. *Adv. Funct. Mater.* **2020**, *30*, 1910718. [[CrossRef](#)]
8. Han, W.B.; Lee, J.H.; Shin, J.-W.; Hwang, S.-W. Advanced Materials and Systems for Biodegradable, Transient Electronics. *Adv. Mater.* **2020**, *32*, 2002211. [[CrossRef](#)]
9. Williams, N.X.; Bullard, G.; Brooke, N.; Therien, M.J.; Franklin, A.D. Printable and recyclable carbon electronics using crystalline nanocellulose dielectrics. *Nat. Electron.* **2021**, *4*, 261–268. [[CrossRef](#)]
10. Lee, D.-M.; Rubab, N.; Hyun, I.; Kang, W.; Kim, Y.-J.; Kang, M.; Choi, B.; Kim, S.-W. Ultrasound-mediated triboelectric nanogenerator for powering on-demand transient electronics. *Sci. Adv.* **2022**, *8*, abl8423. [[CrossRef](#)]
11. Tat, T.; Libanori, A.; Au, C.; Yau, A.; Chen, J. Advances in triboelectric nanogenerators for biomedical sensing. *Biosens. Bioelectron.* **2021**, *171*, 112714. [[CrossRef](#)] [[PubMed](#)]
12. Luo, M.; Martinez, A.W.; Song, C.; Herrault, F.; Allen, M.G. A Microfabricated Wireless RF Pressure Sensor Made Completely of Biodegradable Materials. *J. Microelectromechanical Syst.* **2013**, *23*, 4–13. [[CrossRef](#)]
13. Wang, Y.; Su, Y.; Zhang, Y.; Chen, M. High-Voltage Wave Induced a Unique Structured Percolation Network with a Negative Gauge Factor. *ACS Appl. Mater. Interfaces* **2022**, *14*, 5661–5672. [[CrossRef](#)] [[PubMed](#)]
14. Rotbaum, Y.; Puiu, C.; Rittel, D.; Domingos, M. Quasi-static and dynamic in vitro mechanical response of 3D printed scaffolds with tailored pore size and architectures. *Mater. Sci. Eng. C* **2019**, *96*, 176–182. [[CrossRef](#)] [[PubMed](#)]
15. Chang, K.B.; Parashar, P.; Shen, L.C.; Chen, A.R.; Huang, Y.T.; Pal, A.; Lim, K.C.; Wei, P.H.; Kao, F.C.; Hu, J.J.; et al. A tribo-electric nanogenerator-based tactile sensor array system for monitoring pressure distribution inside prosthetic limb. *Nano Energy* **2023**, *111*, 108397. [[CrossRef](#)]

16. Du, J.; Armstrong, S.R.; Baer, E. Co-extruded multilayer shape memory materials: Comparing layered and blend architectures. *Polymer* **2013**, *54*, 5399–5407. [[CrossRef](#)]
17. Moore, M.J.; Lam, Y.T.; Santos, M.; Tan, R.P.; Yang, N.; Hung, J.; Li, Z.; Kilian, K.A.; Rnjak-Kovacina, J.; Pitts, J.B.; et al. Evaluation of the Immune Response to Chitosan-graft-poly(caprolactone) Biopolymer Scaffolds. *ACS Biomater. Sci. Eng.* **2023**, *9*, 3320–3334. [[CrossRef](#)]
18. Gniesmer, S.; Brehm, R.; Hoffmann, A.; De Cassan, D.; Menzel, H.; Hoheisel, A.-L.; Glasmacher, B.; Willbold, E.; Reifenrath, J.; Wellmann, M.; et al. In vivo analysis of vascularization and biocompatibility of electrospun polycaprolactone fibre mats in the rat femur chamber. *J. Tissue Eng. Regen. Med.* **2019**, *13*, 1190–1202. [[CrossRef](#)]
19. Jing, X.; Mi, H.-Y.; Wang, X.-C.; Peng, X.-F.; Turng, L.-S. Shish-Kebab-Structured Poly(ϵ -Caprolactone) Nanofibers Hierarchically Decorated with Chitosan–Poly(ϵ -Caprolactone) Copolymers for Bone Tissue Engineering. *ACS Appl. Mater. Interfaces* **2015**, *7*, 6955–6965. [[CrossRef](#)]
20. Shen, J.; Yuan, W.; Badv, M.; Moshaverinia, A.; Weiss, P.S. Modified Poly(ϵ -caprolactone) with Tunable Degradability and Improved Biofunctionality for Regenerative Medicine. *ACS Mater. Au* **2023**, *3*, 540–547. [[CrossRef](#)]
21. Lönnberg, H.; Larsson, K.; Lindström, T.; Hult, A.; Malmström, E. Synthesis of polycaprolactone-grafted microfibrillated cel-lulose for use in novel bionanocomposites—influence of the graft length on the mechanical properties. *ACS Appl. Mater. Interfaces* **2011**, *3*, 1426–1433. [[CrossRef](#)]
22. Peterson, G.; Larsen, M.; Ganter, M.; Storti, D.; Boydston, A. 3D-printed mechanochromic materials. *ACS Appl. Mater. Interfaces* **2014**, *7*, 577–583. [[CrossRef](#)]
23. Azari, A.; Golchin, A.; Maymand, M.M.; Mansouri, F.; Ardeshiryajimi, A. Electrospun Polycaprolactone Nanofibers: Current Research and Applications in Biomedical Application. *Adv. Pharm. Bull.* **2022**, *12*, 658–672. [[CrossRef](#)]
24. Wasserscheid, P.; Keim, W. Ionic liquids—New ‘solutions’ for transition metal catalysis. *Angew. Chem.—Int. Ed.* **2000**, *39*, 3772–3789. [[CrossRef](#)]
25. Plechkova, N.V.; Seddon, K.R. Applications of ionic liquids in the chemical industry. *Chem. Soc. Rev.* **2008**, *37*, 123–150. [[CrossRef](#)]
26. Macfarlane, D.R.; Tachikawa, N.; Forsyth, M.; Pringle, J.M.; Howlett, P.C.; Elliott, G.D.; Davis, J.H.; Watanabe, M.; Simon, P.; Angell, C.A. Energy applications of ionic liquids. *Energy Environ. Sci.* **2014**, *7*, 232–250. [[CrossRef](#)]
27. Singh, S.K.; Savoy, A.W. Ionic liquids synthesis and applications: An overview. *J. Mol. Liq.* **2020**, *297*, 112038. [[CrossRef](#)]
28. Zhao, Z.; Hu, Y.-P.; Liu, K.-Y.; Yu, W.; Li, G.-X.; Meng, C.-Z.; Guo, S.-J. Recent Development of Self-Powered Tactile Sensors Based on Ionic Hydrogels. *Gels* **2023**, *9*, 257. [[CrossRef](#)] [[PubMed](#)]
29. Dobashi, Y.; Yao, D.; Petel, Y.; Nguyen, T.N.; Sarwar, M.S.; Thabet, Y.; Ng, C.L.W.; Glitz, E.S.; Nguyen, G.T.M.; Plesse, C.; et al. Piezoionic mechanoreceptors: Force-induced current generation in hydrogels. *Science* **2022**, *376*, 502–507. [[CrossRef](#)] [[PubMed](#)]
30. Heng, W.; Solomon, S.; Gao, W. Flexible Electronics and Devices as Human–Machine Interfaces for Medical Robotics. *Adv. Mater.* **2022**, *34*, 2107902. [[CrossRef](#)] [[PubMed](#)]
31. Fakharuddin, A.; Li, H.; Giacomo, F.; Zhang, T.; Gasparini, N.; Elezzabi, A.; Mohanty, A.; Ramadoss, A.; Ling, J.; Vasilopoulou, M. Fiber-shaped electronic devices. *Adv. Energy Mater.* **2021**, *11*, 2101443. [[CrossRef](#)]
32. Li, F.; Cai, X.; Liu, G.; Xu, H.; Chen, W. Piezoionic SnSe Nanosheets-Double Network Hydrogel for Self-Powered Strain Sensing and Energy Harvesting. *Adv. Funct. Mater.* **2023**, *33*, 2300701. [[CrossRef](#)]
33. Odent, J.; Baleine, N.; Biard, V.; Dobashi, Y.; Vancaeyzeele, C.; Nguyen, G.T.M.; Madden, J.D.W.; Plesse, C.; Raquez, J. 3D-Printed Stacked Ionic Assemblies for Iontronic Touch Sensors. *Adv. Funct. Mater.* **2022**, *33*, 2210485. [[CrossRef](#)]
34. Li, M.; Qiao, J.; Zhu, C.; Hu, Y.; Wu, K.; Zeng, S.; Yang, W.; Zhang, H.; Wang, Y.; Wu, Y.; et al. Gel-Electrolyte-Coated Carbon Nanotube Yarns for Self-Powered and Knittable Piezoionic Sensors. *ACS Appl. Electron. Mater.* **2021**, *3*, 944–954. [[CrossRef](#)]
35. Homayounfar, S.; Kiaghadi, A.; Ganesan, D.; Andrew, T. Pressure: An all-fabric piezoionic pressure sensor for extracting physiological metrics in both static and dynamic contexts. *J. Electrochem. Soc.* **2021**, *168*, 017515. [[CrossRef](#)]
36. Chen, Z.; Wang, Y. Ionic skin: From imitating natural skin to beyond. *Ind. Chem. Mater.* **2023**, *1*, 224–239. [[CrossRef](#)]
37. Bhardwaj, N.; Kundu, S.C. Electrospinning: A fascinating fiber fabrication technique. *Biotechnol. Adv.* **2010**, *28*, 325–347. [[CrossRef](#)] [[PubMed](#)]
38. Agarwal, S.; Wendorff, J.H.; Greiner, A. Use of electrospinning technique for biomedical applications. *Polymer* **2008**, *49*, 5603–5621. [[CrossRef](#)]
39. Deng, Y.; Lu, T.; Cui, J.; Samal, S.K.; Xiong, R.; Huang, C. Bio-based electrospun nanofiber as building blocks for a novel eco-friendly air filtration membrane: A review. *Sep. Purif. Technol.* **2021**, *277*, 119623. [[CrossRef](#)]
40. Di Pasquale, G.; Graziani, S.; Pollicino, A.; Trigona, C. Performance Characterization of a Biodegradable Deformation Sensor Based on Bacterial Cellulose. *IEEE Trans. Instrum. Meas.* **2020**, *69*, 2561–2569. [[CrossRef](#)]
41. Di Pasquale, G.; Graziani, S.; Pollicino, A.; Trigona, C. Green Inertial Sensors based on Bacterial Cellulose. In Proceedings of the SAS IEEE Sensors Applications Symposium, Sophia Antipolis, France, 11–13 March 2019; p. 8706112.
42. Caponetto, R.; Di Pasquale, G.; Graziani, S.; Murgano, E.; Pollicino, A. Realization of green fractional order devices by using bacterial cellulose. *AEU—Int. J. Electron. Commun.* **2019**, *112*, 152927. [[CrossRef](#)]
43. Kurukunda, S.; Graziani, S.; Trigona, C.; Di Pasquale, G.; Pollicino, A.; Pöhako-Esko, K.; Aabloo, A. A Comparative Investigation of Deformation Transducers Based on Bacterial Cellulose and Different Ionic Liquids. In Proceedings of the 2023 IEEE International Instrumentation and Measurement Technology Conference (I2MTC), Kuala Lumpur, Malaysia, 22–25 May 2023; pp. 1–5.

44. McEwen, A.B.; Ngo, H.L.; LeCompte, K.; Goldman, J.L. Electrochemical Properties of Imidazolium Salt Electrolytes for Electrochemical Capacitor Applications. *J. Electrochem. Soc.* **1999**, *146*, 1687–1695. [[CrossRef](#)]
45. Persenaire, O.; Alexandre, M.; Degée, P.; Dubois, P. Mechanisms and Kinetics of Thermal Degradation of Poly(ϵ -caprolactone). *Biomacromolecules* **2001**, *2*, 288–294. [[CrossRef](#)] [[PubMed](#)]

Disclaimer/Publisher’s Note: The statements, opinions and data contained in all publications are solely those of the individual author(s) and contributor(s) and not of MDPI and/or the editor(s). MDPI and/or the editor(s) disclaim responsibility for any injury to people or property resulting from any ideas, methods, instructions or products referred to in the content.